J Mar Sci Technol (2006) 11:88–99
DOI 10.1007/s00773-006-0215-8

Journal of
Marine Science and Technology

Study on the maneuverability of a large vessel installed with a mariner type Super VecTwin rudder

Kazuhiko Hasegawa[1], Donghoon Kang[1], Masaaki Sano[1], and Kenjiro Nabeshima[2]

[1] Department of Naval Architecture and Ocean Engineering, Graduate School of Engineering, Osaka University, 2-1 Yamadaoka, Suita 565-0871, Japan
[2] Japan Hamworthy Co., Ltd., Osaka, Japan

Abstract The suitability of the Mariner type Super VecTwin rudder (hereinafter, the MSV rudder) for a large vessel is assessed in this article. Several experiments in a maneuvering pond were carried out and their results analyzed and summarized. Free-running tests such as turning, zigzag, and stopping tests were carried out with a 4-m free-running model of a very large crude carrier (VLCC) ship with the MSV rudder and the Mariner rudder. The results were compared to validate the maneuverability of a VLCC-sized a ship installed with the MSV rudder. A mathematical model of an MSV rudder is proposed for maneuvering simulation of a large vessel. To develop a maneuvering simulation for the model ship that was used in the free-running tests, hydrodynamic coefficients were estimated based on Kijima's regression formula. The coefficients of interaction between the hull and rudder (t_R, a_H, x_H) were obtained from a self-propulsion test in a towing tank. The complicated flow around the rudders is simplified to model the flow speed around the rudders. This simplified flow speed is utilized to compare the time histories of the free-running tests with the simulations. The mathematical model of the MSV rudder was further improved using the results of this comparison.

Key words Mariner type Super VecTwin rudder · Mathematical model · Maneuverability · Free-running test

List of symbols

a_H	ratio of hydrodynamic force induced on ship hull by rudder action to rudder force
A_R	rudder area
C_b	block coefficient
C_{R1}, C_{R2}	rudder normal force coefficients
C_{RS}, C_{RP}	coefficients of inflow velocity for starboard and port rudders, respectively
$C_{TM} = R(u)\Big/\frac{1}{2}\rho S_W U^2$	coefficient of total resistance
d	ship draft
D_P	propeller diameter
F_n	nominal Froude number
F_{NS}, F_{NP}	rudder normal force for starboard and port rudders, respectively
h_R	rudder height
g	gravitational acceleration
I_{zz}	yaw moment of inertia
J_{zz}	added yaw moment of inertia
K'	Nomoto's index, which is related to turning ability
L	ship length
m	ship mass
m_x	added mass in surge
m_y	added mass in sway
n	propeller revolutions
N_H, N_R	yaw moment of hull and rudder acting on ship
N'_β, N'_r, $N'_{\beta\beta}$, N'_{rr}, $N'_{\beta\beta r}$, $N'_{\beta rr}$	derivatives of yaw moment
O	ship's center of gravity
r	yaw rate
r'_m	nondimensional mean angular velocity as defined by Nomoto for the zigzag test
$R(u)$	ship resistance
S_W	wetted surface area
T'	Nomoto's index, which is related to course stability
t_P	thrust deduction factor
t_R	coefficient for additional drag of rudder
u	surge velocity
U	ship velocity
v	sway velocity
x_H	ratio of hydrodynamic moment induced on ship hull by rudder action to rudder force
x_P	x coordinate of propeller location
x_R	x coordinate of rudder location
X_H, X_P, X_R	x-axis components of hull, propeller, and rudder force acting on ship

Address correspondence to: D.H. Kang
(Kang_Dong_Hoon@naoe.eng.osaka-u.ac.jp)
Received: August 2, 2005 / Accepted: January 5, 2006

X'_{vr}	derivative of surge force
Y_H, Y_R	y-axis components of hull and rudder force acting on ship
Y'_β, Y'_r, $Y'_{\beta\beta}$, Y'_{rr}, $Y'_{\beta\beta r}$, $Y'_{\beta rr}$	derivatives of sway force
α_{RS}, α_{RP}	starboard and port effective rudder inflow angle
β	drift angle
δ_S, δ_P	starboard and port rudder angles
ε	wake ratio between propeller and rudder
η	ratio of propeller diameter by rudder height
κ	parameter with rudder inflow velocity
ρ	water density
γ_R	flow straightening factor
ω_{P0}	effective wake fraction in straight runnings

1 Introduction

Blunt body ships such as very large crude carriers (VLCC) have more resistance and lower maneuverability as compared to fine form ships, because of their hull form which is designed for higher loading and low speed. Many efforts have been made to overcome the defects due to inherent design of these ships. Optimizing hull form for reducing the resistance is one such example, which increases propulsion ability,[1] but it is difficult to assert that the optimized hull form by itself increases ship's maneuverability. In some cases, on the contrary, the hull designed for better propulsion ability may decrease ship's maneuverability. Utilizing special controller is another such example of increasing ship's maneuverability.[2] Even though these special control systems perform excellently in certain circumstances, it does not mean that they can increase the inherent maneuverability of a ship. Using special rudder systems is one such alternative for increasing the inherent maneuverability of such vessels. In this paper, a special rudder system which can be adapted to these vessels is introduced and studied.

Some existing design of large sized vessels such as VLCCs, which have been well proven, are now in contravention of the IMO Standards for ship maneuverability,[3] especially stopping ability. Small and middle-sized vessels installed with a Super VecTwin rudder (hereinafter, the SV rudder) show better stopping ability and maneuverability than those installed with a conventional rudder. Although it is expected that an SV rudder system for a large vessel would also be able to improve their maneuverability and stopping ability by controlling two rudders, until now no large vessel has been installed with an SV rudder. This is because using SV rudders on large vessels necessitates, large diameter rudder stocks and a special design of stern.[4] Consequently, the propulsive performance would be lower as a result of the thicker rudder profile from the bigger rudder stock diameter. Therefore, a Mariner type Super VecTwin rudder (hereinafter, the MSV rudder) has been discussed to solve the above problem.

In this article, the maneuverability of a large vessel installed with an MSV rudder is validated by carrying out several experiments in a maneuvering pond. Free-running tests of the VLCC model ship with an MSV rudder and a Mariner rudder were carried out. The above tests were compared to assess the suitability of the MSV rudder to a large vessel.

Furthermore, a mathematical model for an MSV rudder was initially developed based on the mathematical modeling group (MMG) model to carry out maneuvering simulation for a large vessel. This model was further improved after comparing the results of simulations and free-running tests. To improve this model, the complicated flow speed pattern behind the propeller is simplified to the mean flow speed around the rudders. Time histories of the free-running test were compared with those of simulations to estimate the mean flow speed around the rudders. Furthermore, a method for asymmetrically positioning the MSV rudders with respect to the ship's centerline, so as to achieve a symmetric maneuvering motion is explained. It should be noted that the above method cannot be directly applied to other vessels. This is because the mathematical model of the rudder is suitable only for the VLCC model studied in this article. However, since the applied method is based on the MMG model, it can be used for other vessels with a few modifications such as by tuning the coefficients of the rudder model.

2 Model ship

A 4-m free-running VLCC model ship was chosen for this study; the particulars of the model are shown in Table 1. The model is equipped with a detachable type of stern that can be changed to suit various types of rudder. Two types of rudder, the MSV rudder and the Mariner rudder, were used for the experiment. The total area of the MSV rudder is less than that of the Mariner rudder because the cross section of each MSV rudder is similar to that of a Schilling rudder and therefore has a higher lift coefficient than that of the Mariner rudder. The main dimensions of the rudders are shown in Table 2.

It is well known that ships equipped with VecTwin rudders exhibit excellent maneuverability, especially while approaching and departing from a pier.[5] The SV rudder is a new design concept in which horizontal fins

are added to a VecTwin rudder. By employing horizontal fins, the rotational energy of the propeller slipstream is converted to linear kinetic energy; thereby an improvement in the overall propulsive efficiency of the ship is expected. However, despite the above-mentioned benefits, no large vessel has been installed with a VecTwin rudder or an SV rudder. This is because these rudders have no pintle bearings and therefore require a larger-diameter rudder stock and a special design for the stern so as to sustain the heavy bending moments from the rudder lifting forces. Consequently the propulsive performance compared to a Mariner rudder is slightly reduced because of the thicker rudder profile. Therefore, the MSV rudder has been discussed as a possible solution to the above problem. The cross section and rudder profile of the MSV rudder is the same as that for the SV rudder, including the horizontal fins. The SV rudder system is classified as a spade rudder (without a rudder horn), and the MSV rudder is classified as a semispade rudder (with a rudder horn). In the MSV rudder, the main addition is a rudder horn, similar to the rudder horn used for the Mariner rudder. This additional rudder horn is used for housing a bearing, which in turn takes the load from an additional "horn pintle" provided for the MSV rudder. This arrangement reduces the loading on the rudder stock, and thereby its diameter, to permissible levels, thus making the design feasible for large vessels. Rudder thickness is also reduced because of the lower stock diameter. A typical MSV type rudder is shown in Fig. 1.

3 Experiment for validating the MSV rudder

Several free-running tests were carried out to validate the maneuverability of a VLCC ship model installed with an MSV rudder. During the experiment the heading angle of the ship was measured by gyroscope and its trajectories measured by an RTK GPS (Trimble, CA, USA) that has an accuracy of ± 0.03 m. Both the instruments were installed on board the model. Table 3 lists the turning, zigzag, and stopping tests carried out with the model ship with the MSV rudder and the Mariner rudder. All the tests commenced at an initial speed of 0.8 m/s, which corresponds to a full-scale speed of 13.5 knots for a 300-m-long VLCC. Speed tests with both types of rudder were performed in the maneuvering pond. The revolutions of the stock propeller (hereinafter, rps) were set at 14.2 when using the MSV rudder and at 13.7 when using the Mariner rudder. The model speed corresponding to these rps values was 0.8 m/s. From the above, it is observed that the MSV rudder increases the ship's drag compared with the Mariner rudder. However, it must be noted that the scaling factor for the increased drag as a result of the rudder is still a matter of debate. The scaling factor is expected to be less compared to what is normally applied for the ship's resistance. Furthermore in the case of the MSV rudder, there is an increase in drag caused by the propeller hub vortex; however, this can be reduced by various means, for example, by using a propeller boss cap fin, although there is some debate on this matter also. Hence, for a full-scale ship, this matter warrants further study before any firm conclusions can be drawn.

3.1 Stopping tests (crash stop astern)

This test was carried out for the model ship both with the MSV rudder and the Mariner rudder. The following procedure for emergency stopping was carried out for each run. After the order for stopping was given, the

Table 1. Principal dimensions of the model ship

L	4.00 m	X_G	0.123 m
B	0.667 m	S_W	4.049 m^2
d	0.240 m	D_P	0.12057 m
C_b	0.817	P/D_P	0.6669

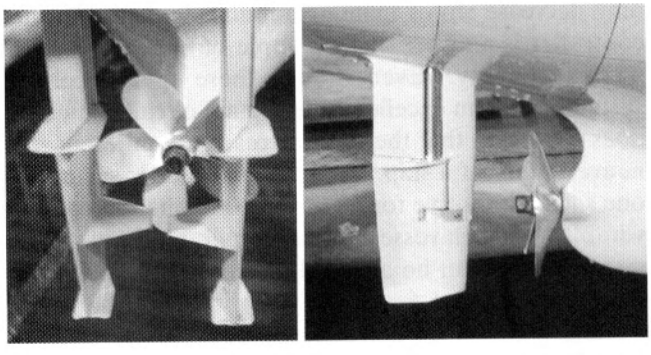

Fig. 1. Shape of Mariner type Super VecTwin (MSV) rudder

Table 2. Main dimensions of the rudders

Dimension	Mariner rudder	MSV rudder	Remarks
Height of rudder (m)	0.169	0.116	
Breadth of rudder (m)	0.1175/0.09	0.081/0.0565	Top/bottom
A_R (m^2)	0.01468	0.00672 × 2	Effective rudder area
A_R/Ld	1/65.4	1/71.0	

MSV, Mariner type Super VecTwin

propeller speed was reduced in steps until it became zero, then the propeller was reversed until the ship's ahead speed was zero. In the case of the MSV rudder, it is well known that the total resistance of a ship increases by positioning the two rudders like an open clam shell. To find the optimum rudder angles required for stopping with the MSV rudder with a certain initial speed, self-propulsion tests with the rudders in the open clam shell position were carried out in a towing tank. The rudder angles were set such that the hinged position of the open clam shell was near the propeller. Three different sets of rudder angles were investigated, i.e., ±30°, ±60°, and ±80°. The results are shown in Fig. 2, where it can be seen that with increasing rudder angles, the total resistance increases; however, the increase in resistance beyond a 60° rudder angle was not significant. Moreover, increased rudder angles cause an increase in steering gear torque. Hence, for an initial speed of 0.8 m/s, a ±60° rudder angle was set for the stopping test. Three different procedures for the stopping tests were followed for the MSV rudder. Figure 3 shows the stopping procedures with the Mariner and the MSV rudders and Figs. 4 and 5 show the trajectory and track reach, re-

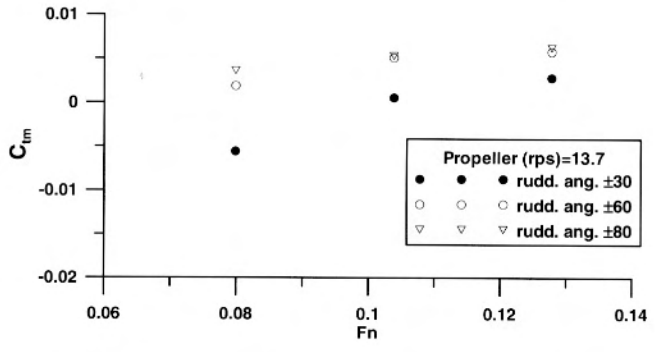

Fig. 2. Resistance tests of the MSV rudder in open clam shell configuration. *Rudd. ang.*, rudder angle; *rps*, revolutions per second

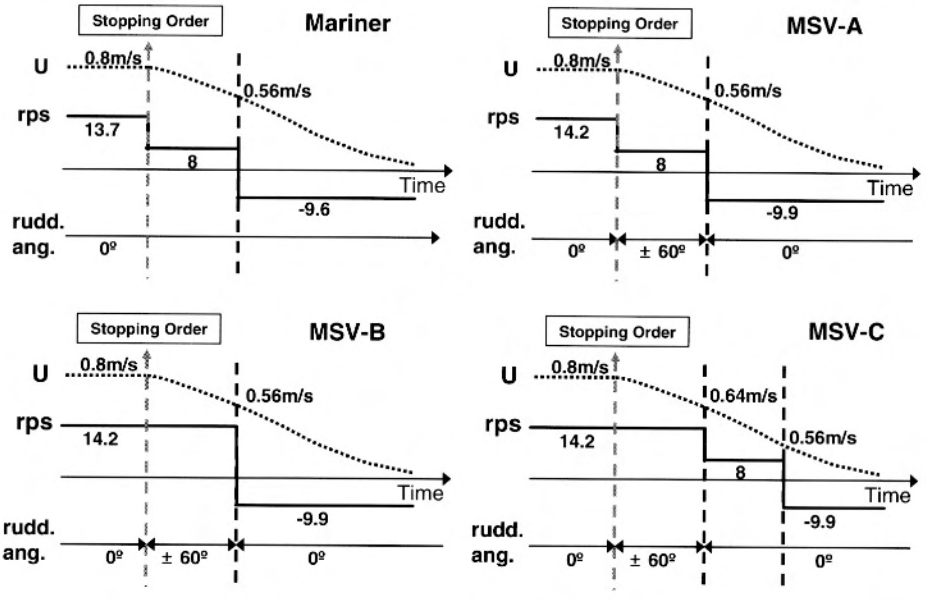

Fig. 3. Procedures of for the stopping test. Three different procedures were used for the MSV rudder

Table 3. Turning, zigzag, and stopping tests carried out

Test	Mariner rudder	MSV rudder	Remarks
Turning test	+35°, −35°	(+15°, +15°), (−15°, −15°), (+15°, +30°), (−30°, −15°), (+30°, +30°), (−30°, −30°), (+30°, +45°), (−45°, −30°), (+30°, +60°), (−60°, −30°)	(Port, starboard)
Zigzag test	+10°, −10°, +15°, −15°, +20°, −20	+5°, −5°, +10°, −10°, +15°, −15°, +20°, −20°	The two MSV rudders are synchronous
Zigzag test with asymmetric rudder angles		+5° (+5°, +7.5°), +5 °(+5°, +10°), −5° (−7.5°, −5°), −5° (−10°, −5°), +10° (+10°, +15°), +10° (+10°, +20°), −10° (−15°, −10°), −10° (−20°, −10°)	(Port, starboard): starting order angle
Stopping test	Refer to Fig. 3	Refer to Fig. 3	

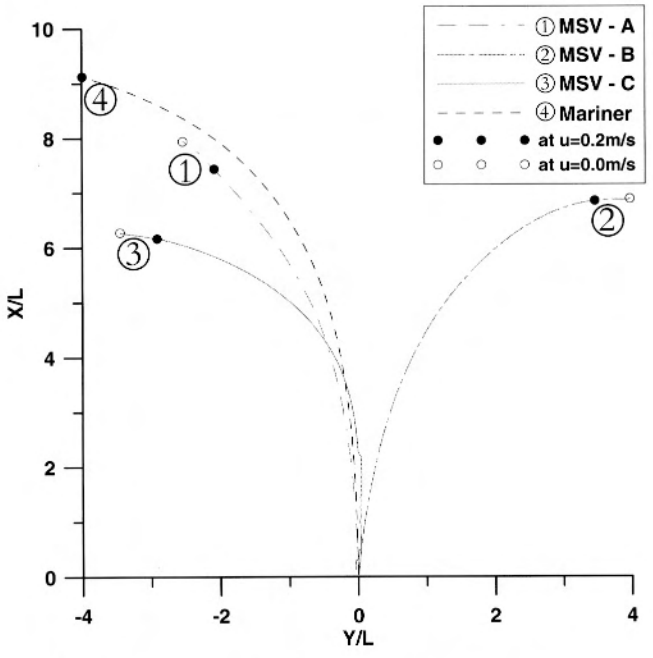

Fig. 4. Trajectories in the stopping test

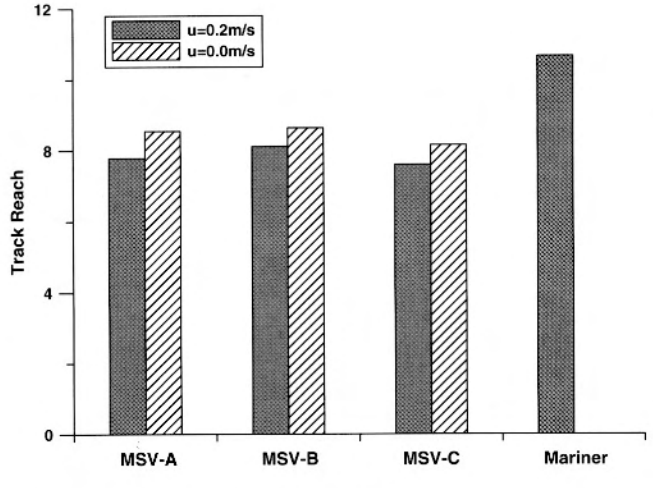

Fig. 5. Track reach of stopping test

spectively, during the stopping test. It should be noted that for all the tests with the MSV rudder, the trajectory and track reach was measured until the ship's ahead speed was 0. But in the case of the Mariner rudder, these data were measured until the ship's ahead speed was 0.2 m/s. In tests on the Mariner rudder, the experiment was terminated at a ship ahead speed of 0.2 m/s because of the limited size of the available facility. It was observed that for all the stopping tests with the MSV rudder, the track reach was shorter than that with the Mariner type rudder.

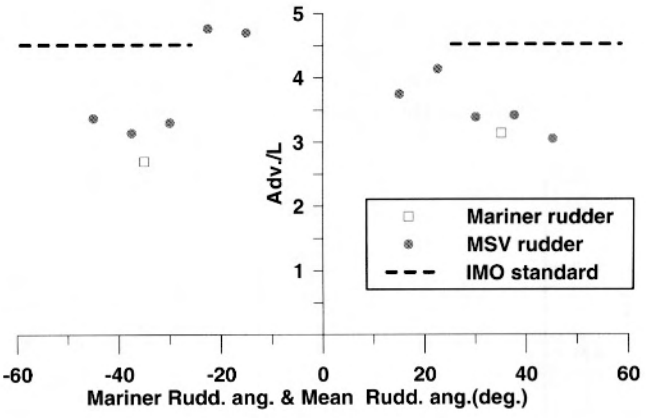

Fig. 6. Comparison of the advance (*Adv*) in turning tests between the MSV rudder and the Mariner rudder

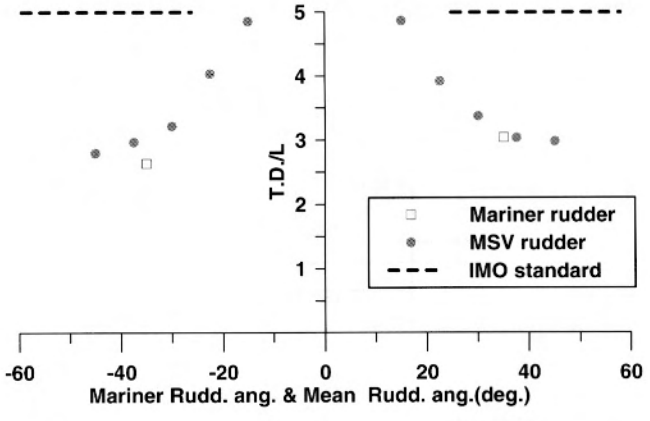

Fig. 7. Comparison of the tactical diameter (*TD*) in turning tests between the MSV rudder and the Mariner rudder

3.2 Turning tests

Figures 6 and 7 show the advance and tactical diameter, respectively, of the model ship with the MSV rudder and the Mariner rudder. For the MSV rudder, the mean rudder angle means the average of the port and starboard rudder angles. It is noted that the ship with the Mariner rudder has a better turning ability, but the ship with the MSV rudder has a turning ability that meets IMO standards, even at small rudder angles.

3.3 Zigzag tests

Zigzag tests were performed at 10°, 15°, and 20° to check the course stability of the model ship. Nomoto's indexes[6] K' and T' were plotted as functions of r'_m, in Figs. 8 and 9. It is well known that K' demonstrates the turning ability of a ship and T' demonstrates the course stability. Generally, the ship with the Mariner rudder had better turning ability and course stability than the

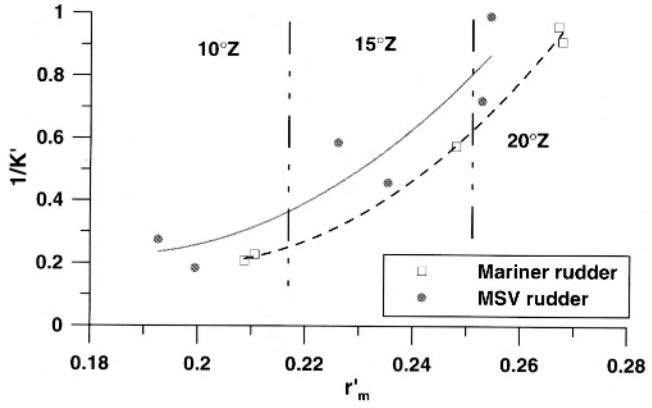

Fig. 8. Comparison of K' in zigzag tests between the MSV rudder and the Mariner rudder

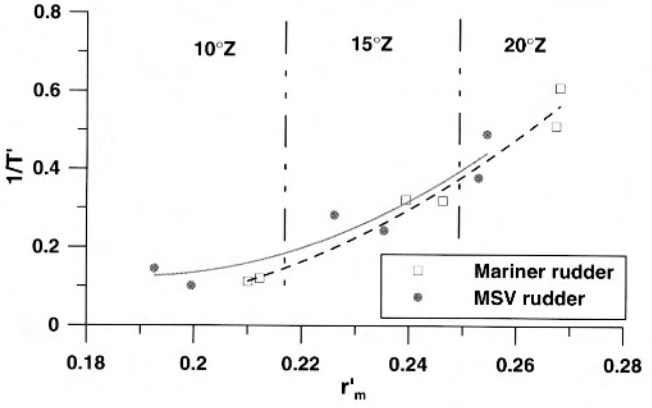

Fig. 9. Comparison of T' in zigzag tests between the MSV rudder and the Mariner rudder

ship with the MSV rudder, but the difference was not significant.

In all the above experiments, it can be seen that for the same rudder area, the ship with the MSV rudder shows sufficient maneuverability, especially when stopping. However, the MSV rudder area can be further increased because sufficient space is available between the rudder bottom and ship's keel. Increasing the rudder area will further improve the ship's maneuverability. For the Mariner rudder, there is no space to increase the rudder area; the respective positions of the Mariner rudder and the MSV rudder are shown in Fig. 10. It should be noted that the rudder horn for both rudders has been omitted in the drawing for ease of comparison.

4 Mathematical model

The suitability of the MSV rudder to a VLCC is addressed in Sect. 3, but the tests done in thus section do not indicate its applicability to other types of large vessels. Using a mathematical model of the MSV rudder is one

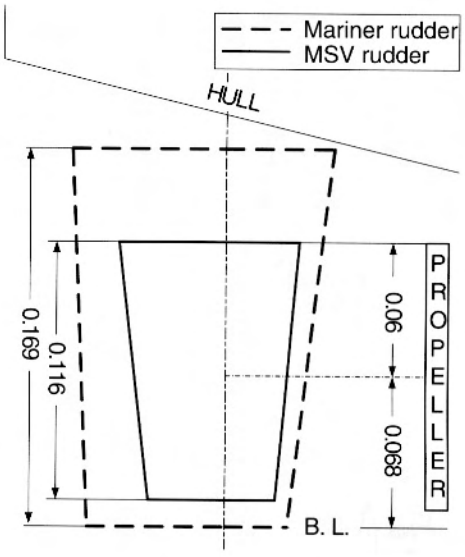

Fig. 10. Positions of the Mariner and the MSV rudders (units are in millimeters)

method to assess its suitability for other large vessels. The mathematical model for the MSV rudder was developed based on the MMG model,[7] considering the above requirement. The model was further improved by comparing the results of simulations and free-running tests.

4.1 Equations of motion

The mathematical model of the ship maneuvering motion is expressed as:

$$\begin{aligned}
&\left(m+m_x\right)\dot{u}-\left(m+m_y\right)vr = X_H + X_P + X_R \\
&\left(m+m_y\right)\dot{v}+\left(m+m_x\right)ur = Y_H + Y_R \\
&\left(I_{zz}+J_{zz}\right)\dot{r} = N_H + N_R
\end{aligned} \tag{1}$$

The coordinate system is shown in Fig. 11.

4.2 Hull forces and moment

The longitudinal force X_H, lateral force Y_H, and yaw moment N_H, acting on the ship hull are expressed as follows:

$$\begin{aligned}
X_H &= \frac{1}{2}\rho LdU^2\left(X'_{vr}v'r'\right)+R(u) \\
Y_H &= \frac{1}{2}\rho LdU^2\left(Y'_\beta\beta+Y'_r r'+Y'_{\beta\beta}\beta|\beta|+Y'_{rr}r'|r'|\right. \\
&\quad \left.+\left(Y'_{\beta\beta r}\beta+Y'_{\beta rr}r'\right)\beta r'\right) \\
N_H &= \frac{1}{2}\rho L^2dU^2\left(N'_\beta\beta+N'_r r'+N'_{\beta\beta}\beta|\beta|+N'_{rr}r'|r'|\right. \\
&\quad \left.+\left(N'_{\beta\beta r}\beta+N'_{\beta rr}r'\right)\beta r'\right)
\end{aligned} \tag{2}$$

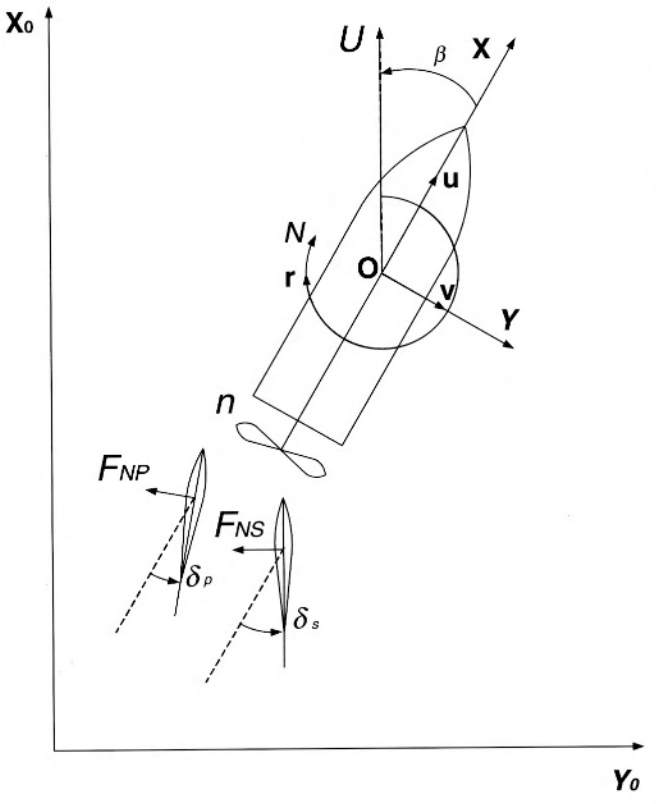

Fig. 11. Coordinate system

$X'_{vr}v'r'$ is predicted using the Hasegawa chart[8] and $R(u)$ of the ship with the MSV rudder is measured from a resistance test in a towing tank. For the lateral force and yaw moment, the hydrodynamic coefficients relative to β, Y'_{β}, $Y'_{\beta\beta}$, N'_{β}, and $N'_{\beta\beta}$ are measured in a towing tank, while the others are estimated based on Kijima's regression formula.[9]

4.3 Propeller force

The hydrodynamic force as a result of the propeller was measured by a self-propulsion test in a towing tank and can be written as follows:

$$X_P = (1-t_P)\rho n^2 D_P^4 K_T(J_P) \tag{3}$$

Where

$$\begin{aligned} K_T(J_P) &= C_1 + C_2 J_P + C_3 J_P^2 \\ J_P &= U\cos\beta(1-\omega_P)/(nD_P) \\ \omega_P &= \omega_{P0}\left\{1-(1-\cos^2\beta_P)(1-|\beta_P|)\right\} \\ \beta_P &= \beta - x'_P r' \end{aligned} \tag{4}$$

4.4 Rudder forces and moment

To express the hydrodynamic forces and moment caused by the MSV rudder, Hamamoto's expression[10] is used. These forces and moment are expressed as follows:

$$\begin{aligned} X_R &= -(1-t_R)(F_{NS}\sin\delta_S + F_{NP}\sin\delta_P) \\ Y_R &= -(1+a_H)(F_{NS}\cos\delta_S + F_{NP}\cos\delta_P) \\ N_R &= -(x_R + a_H x_H)(F_{NS}\cos\delta_S + F_{NP}\cos\delta_P) \end{aligned} \tag{5}$$

$$F'_{NS} = \frac{F_{NS}}{\frac{1}{2}\rho A_R U_{RS}^2} C_{R1}\tan^{-1}(C_{R2}\alpha_{RS})$$

$$F'_{NP} = \frac{F_{NP}}{\frac{1}{2}\rho A_R U_{RP}^2} C_{R1}\tan^{-1}(C_{R2}\alpha_{RP})$$

$$U_{RS} = \frac{1}{U}\sqrt{u_{RS}^2 + v_{RS}^2}$$

$$U_{RP} = \frac{1}{U}\sqrt{U_{RP}^2 + v_{RP}^2}$$

$$u_{RS} = \frac{\varepsilon u_P}{1-s}\sqrt{1-2(1-\eta\kappa)s + (1-\eta\kappa(2-\kappa))s^2}$$

$$u_{RP} = \frac{\varepsilon u_P}{1-s}\sqrt{1-2(1-\eta\kappa)s + (1-\eta\kappa(2-\kappa))s^2}$$

$$\begin{aligned} u_P &= (1-\omega_P)u \\ \kappa &= kx/\varepsilon \\ \eta &= D_P/h_R \\ s &= 1-u_P/nP \\ v_{RP} &= -\gamma_R(v + Lr\cdot u) \\ v_{RS} &= -\gamma_R(v + Lr\cdot u) \end{aligned} \tag{6}$$

To obtain the coefficients of interaction between hull and rudder (t_R, a_H, x_H), the model ship with the MSV rudder and the propeller was tested in a towing tank.

An open-water test of the MSV rudder was not performed. The normal force acting on the MSV rudder was estimated by considering it to be a Schilling rudder. This is because the cross section of the MSV rudder without a fin is the same as that of a Schilling rudder. In this approximation, the effect of the fin is ignored. The conventional formula for the normal rudder force cannot represent that of a Schilling rudder at large rudder angles beyond the stall; therefore, curve fitting is used to express the rudder normal force acting on the MSV rudder by approximating it to a Schilling rudder.

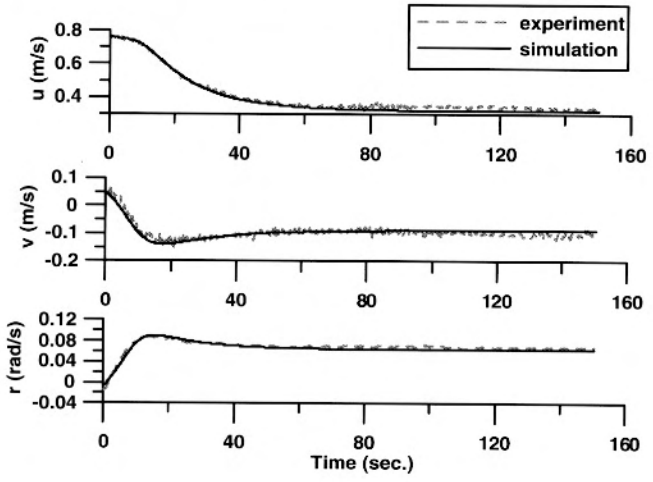

Fig. 12. Comparison of simulation and experiment in the 30° turning test

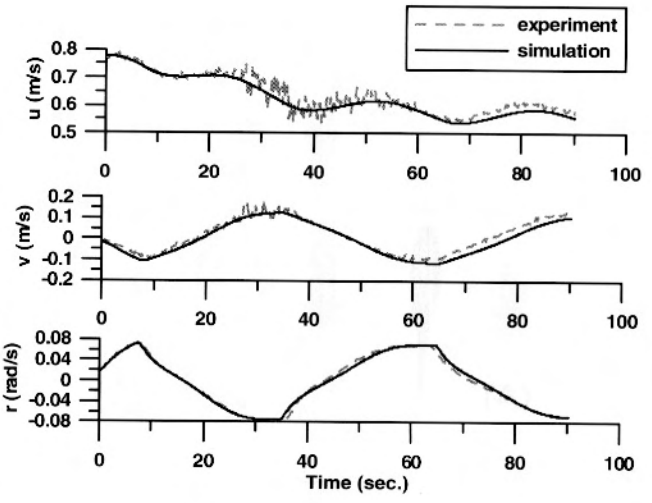

Fig. 13. Comparison of simulation and experiment in the 20° zigzag test

5 Simulation

5.1 Validating the simulation

Simulations with the mathematical model proposed in Sect. 4 were carried out. The results of the simulation were compared with those from the free-running tests carried out in the maneuvering pond. The outline of the simulation is as follows:

1. The initial conditions of the free-running test, such as u, v, and r, were also used for those of the simulation.
2. External forces, including wind, were not considered in the simulation.

The accuracy of the simulation in the incipient stage was confirmed with the ±30° turning test and the ±20° zigzag test. The trajectories and time histories of the simulation agreed closely with the above-mentioned free-running tests. Figures 12 and 13 show comparisons of u, v, and r for simulation and the free-running tests for the 30° turning test and the 20° zigzag test, respectively.

However, the mathematical model could not accurately simulate the free-running tests other than the ±30° turning test and the ±20° zigzag test. Therefore, the mathematical model was further improved, and this is explained in the next section.

5.2 Improving the mathematical model of the MSV rudder

After analyses of the free-running tests, it was noted that the motion of the model ship was highly unsymmetrical for port and starboard turns, even when the MSV rudders were positioned symmetrically about the ship's centerline.

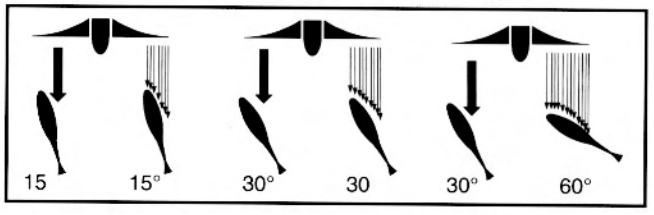

Fig. 14. Images of flow speed around the MSV rudder

For the single Mariner rudder, over the entire range of rudder angles, the rudder is always in the propeller slipstream. In this condition, the flows on the port and starboard sides of the rudder are not the same. It must be noted that this phenomenon results from the rotation of the propeller. This has been well researched for the case of a single propeller and single rudder.[11,12] For the twin MSV rudder, for various rudder angles, the area of the rudder in the propeller slipstream is different, hence the above phenomenon becomes much more significant, as shown in Fig. 14. In the 30°–60° case, the flow on the starboard rudder is greater compared to 15°–15° case. This is because when the leading edge of the rudder moves inboard, it results in the propeller slipstream shifting to the starboard side. Because of this, the usual modeling techniques give erroneous results.

To improve the simulation, a new concept for defining the mean flow around the rudders is proposed. The assumptions and procedures are as follows:

1. The complicated flow behind the propeller is divided into three different mean flows around the rudders. The mean flow is assumed as the average of the flow

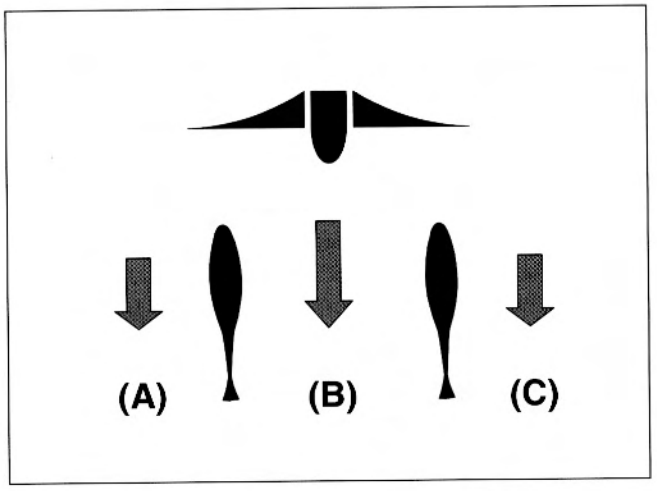

Fig. 15. Concept of the three different mean flows around the rudders

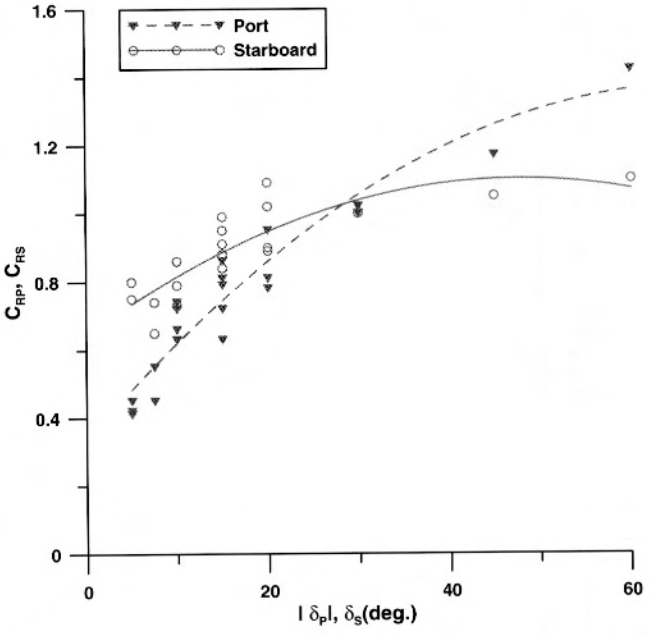

Fig. 16. Ratio of mean flow speed around the port and starboard rudders

over the full depth of the rudder. The flow speeds are defined as (A), (B), and (C) respectively, as shown in Fig. 15. The flow speeds at positions (A) and (C) are different because when the ship is moving ahead, the propeller is rotating clockwise when seen from aft. Two coefficients C_{RS} and C_{RP} are defined, which are used for defining the flow on the starboard and port rudder respectively.

2. The flow speeds around the rudders (u_{RS}, u_{RP}) in Eq. 6 are redefined as follows:

$$u_{RS} = C_{RS}(\delta_s) \times \frac{\varepsilon u_P}{1-s}\sqrt{1-2(1-\eta\kappa)s+(1-\eta\kappa(2-\kappa))s^2}$$
$$u_{RP} = C_{RP}(\delta_p) \times \frac{\varepsilon u_P}{1-s}\sqrt{1-2(1-\eta\kappa)s+(1-\eta\kappa(2-\kappa))s^2} \quad (7)$$

3. In the free-running tests, the turning radii for the +30° and –30° turning tests are similar as compared to turning tests with different rudder angles. So, it is assumed that the flows (A) and (C) are also similar at +30° rudder angle for the starboard rudder and –30° rudder angle for the port rudder. These rudder angles are defined as the reference points. The coefficients of the reference points are defined as follows:

$$C_{RS} = 1.0 \quad \text{at } \delta_s = +30°$$
$$C_{RP} = 1.0 \quad \text{at } \delta_p = -30° \quad (8)$$

4. The values of the coefficients C_{RS} and C_{RP} change with the rudder angle. The effective area of rudder in the propeller slipstream is proportional to the rudder angle. However, the mean flows around the rudder may not change linearly relative to the rudder angle. This is because the flows are also affected by the interaction among the two rudders and the propeller slipstream. The coefficients can be defined as follows:

$$C_{RS}(\delta_s) = C_{RS1}\delta_s^2 + C_{RS2}\delta_s + C_{RS3} \quad \text{at } 0° < \delta_s < 60°$$
$$C_{RP}(\delta_p) = C_{RP1}\delta_p^2 + C_{RP2}\delta_p + C_{RP3} \quad \text{at } -60° < \delta_p < 0° \quad (9)$$

5. The coefficients C_{RS} and C_{RP} are equal to 1.0 whenever the rudder angle is inboard. This is because when the rudders are turned inboard, most of the rudder is in the propeller slipstream. Thus, the coefficients can be defined as follows:

$$C_{RS} = 1.0 \quad \text{at } -30° < \delta_s < 0°$$
$$C_{RP} = 1.0 \quad \text{at } 0° < \delta_p < 30° \quad (10)$$

6. The coefficients C_{RS} and C_{RP} were obtained by comparing results of the simulations and the free-running tests. A trial and error method was used for determining these coefficients. Corresponding to each free-running test, simulations with various assumed values of C_{RS} and C_{RP} were carried out until the results of the simulation matched those of the free-running tests. The values of C_{RS} and C_{RP} thus obtained were plotted against δ_s and δ_p respectively. Based on the above results, Eq. 9 was obtained.

Figure 16 shows the plot of coefficients C_{RS} and C_{RP}. The symbols represent the values obtained by method 6

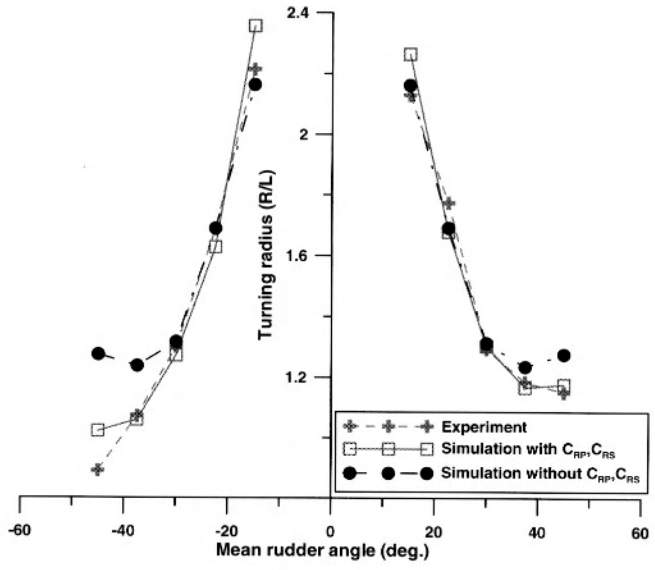

Fig. 17. Comparison of turning radius for experiments and simulations

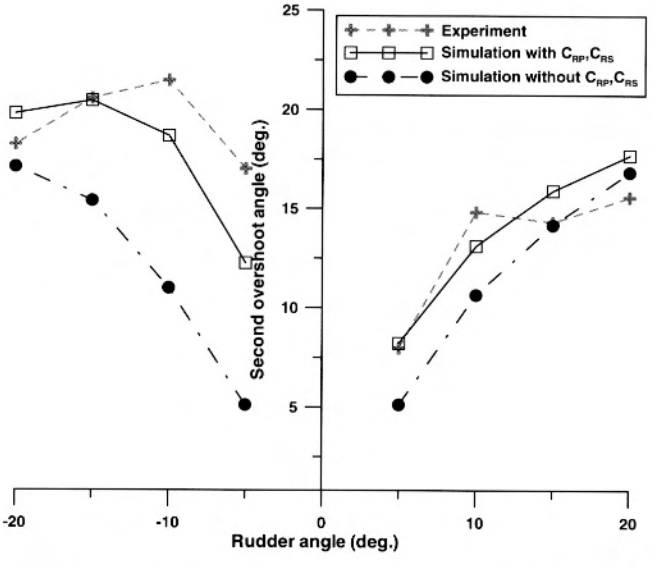

Fig. 18. Comparison of second overshoot angle for experiments and simulations

above. The lines have been obtained by curve fitting using Eq. 9. Figure 17 shows a comparison of the turning radii obtained from the free-running tests and the simulations (with and without the coefficients C_{RS} and C_{RP}). Similarly, Fig. 18 shows a comparison of the second overshoot angle for zigzag tests (hereinafter, the second overshoot). The results of the free-running tests are very asymmetric with respect to the requested rudder angles. However, the simulations without the coefficients C_{RS} and C_{RP} give symmetric results that do not reflect reality. It was observed that simulation results using the coefficients C_{RS} and C_{RP} more accurately express the findings of the free-running tests than the simulation results without these coefficients (Appendix).

Originally, the MSV rudder was located symmetrically about the ship's centerline, but from Figs. 17 and 18, it can be seen that the port and starboard maneuvering are different for such a symmetrical rudder position. For convenience of ship operation, it is desirable that the ship's port and starboard maneuvering characteristics be similar. Several simulations were carried out by positioning the MSV rudder asymmetrically about the ship's centerline. From simulations, it was observed that for a particular asymmetrical position of the MSV rudder, the port and starboard maneuvering became similar. This is explained in detail in the following section.

5.3 Optimization of location of the MSV rudder

In this section, a method of obtaining the off-center distance of the MSV rudder from the ship's centerline is proposed. From Fig. 16, it can be observed that it is impossible to reduce the unsymmetrical maneuvering motion for the entire range of rudder angles. Under normal operating conditions, the helmsman usually sets the rudder angle in the range 10°–20°. Therefore, only 5°–20° zigzag simulations were taken into consideration for this proposal.

The magnitude of the unsymmetrical maneuvering motion, S, is defined as:

$$\begin{aligned} S = &\left|\left(5^\circ \text{ second overshoot}\right) - \left(-5^\circ \text{ second overshoot}\right)\right| \\ &+ \left|\left(10^\circ \text{ second overshoot}\right) - \left(-10^\circ \text{ second overshoot}\right)\right| \\ &+ \left|\left(15^\circ \text{ second overshoot}\right) - \left(-15^\circ \text{ second overshoot}\right)\right| \\ &+ \left|\left(20^\circ \text{ second overshoot}\right) - \left(-20^\circ \text{ second overshoot}\right)\right| \end{aligned} \tag{11}$$

The calculations were made with various off-center positions. The values δ_s and δ_p of the x-axis in Fig. 16 can be alternated with $d_{\delta s}$ and $d_{\delta p}$, which are defined in Fig. 19. The values C_{RS} and C_{RP} were fitted again with the $d_{\delta s}$ and $d_{\delta p}$ values. Equation 9 was modified to become a function of $d_{\delta s}$, $d_{\delta p}$, and Δd_δ for calculating the off-center position Δd_δ of the rudders:

$$\begin{aligned} C'_{RS}\left(d_{\delta s}, \Delta d_\delta\right) &= C'_{RS1}\left(d_{\delta s} + \Delta d_\delta\right)^2 + C'_{RS2}\left(d_{\delta s} + \Delta d_\delta\right) + C'_{RS3} \\ C'_{RP}\left(d_{\delta p}, \Delta d_\delta\right) &= C'_{RP1}\left(d_{\delta p} - \Delta d_\delta\right)^2 + C'_{RP2}\left(d_{\delta p} - \Delta d_\delta\right) + C'_{RP3} \end{aligned} \tag{12}$$

It was noted that there will not be any change in hydrodynamic coefficients of the hull as a result of the shift in

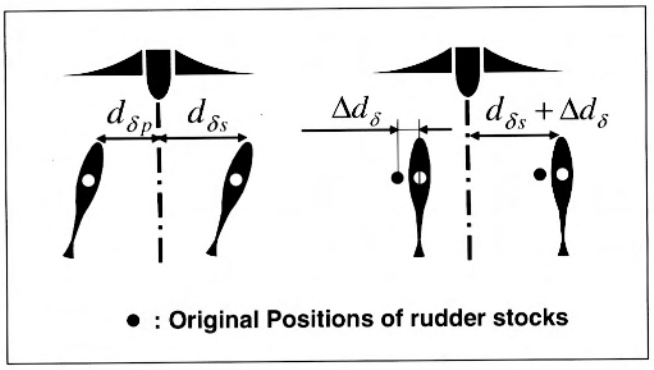

Fig. 19. Definitions of $d_{\delta s}$, $d_{\delta p}$, and Δd_δ for rudder positions asymmetric about the ship's centerline

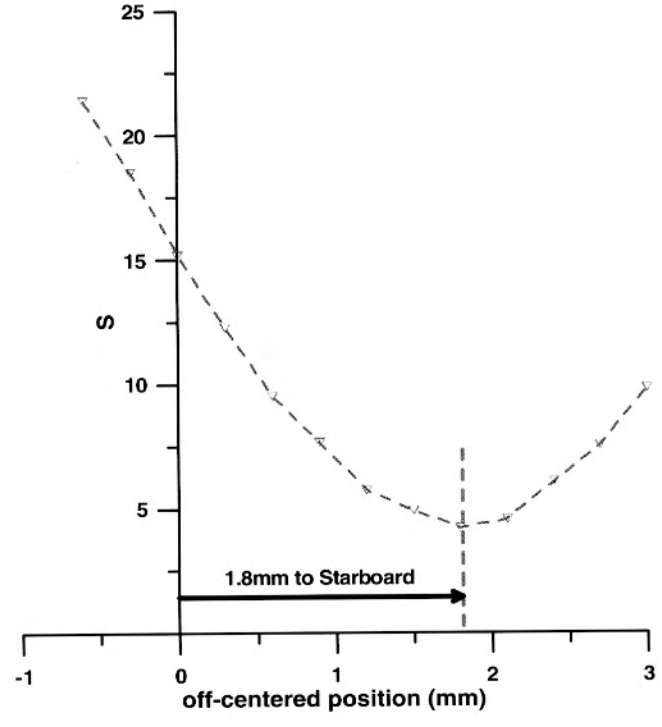

Fig. 20. Optimum position of MSV rudder. S, magnitude of the unsymmetrical maneuvering motion

rudder position. This is because the simulation model was developed based on the MMG model, in which the actions of the rudder, propeller, and hull are considered separately. However, the coefficients of interaction between the hull and rudder (t_R, a_H, x_H) may be changed by the off-center rudder position. For this calculation, it is assumed that these changes are not significant, so the same values of these coefficients were used for all the simulations.

Figure 20 shows the results of the calculations. The smallest S value appears at an off-center location of the rudder 1.8 mm to starboard for the scale model. This represents 2% of the distance between the two rudders.

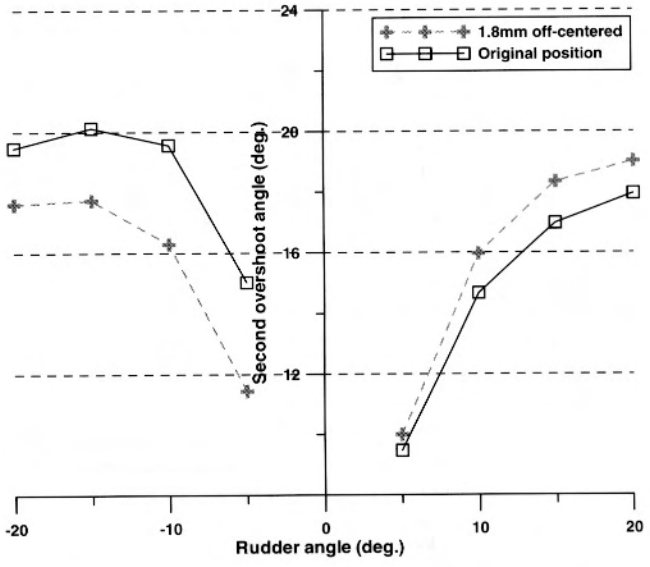

Fig. 21. Comparison of second overshoot angle for simulations at the original position and simulations at the off-center position

Figure 21 shows a comparison of the simulation for the second overshoot between the original rudder position and the 1.8-mm off-center position. Comparing the simulations for both positions, it is observed that with the 1.8-mm off-center position of the MSV rudder, port and starboard maneuvering are almost symmetric.

Large rudder angles were not considered in this proposal. Therefore, even when MSV rudders are asymmetrically located, for rudder angles greater than 20°, the maneuvering motion of the ship to the port and starboard will not be the same. For such a case, the ship master should be provided with data on the expected maneuvering motions to facilitate operation.

Alternatively, if the asymmetric rudder position concept is not used, then a virtual rudder angle concept may be employed. In this concept, the commanded rudder angle given by master and the actual rudder angle are different. The actual rudder movement will be such as to give symmetric maneuvering motions to port and starboard.

6 Conclusions

This paper describes the suitability of an MSV rudder to a large vessel. The suitability is investigated by carrying out free-running tests on a VLCC model ship. An improved mathematical model of the MSV rudder was proposed based on the MMG model, which can also be adapted to other large vessels.

1. In the free-running tests, the model ship with the MSV rudder shows superior stopping ability to the

Table 4. Coefficients used in the simulation

Hull	m'	0.27256	m'_x	0.0177152
	m'_y	0.209845	I'_{zz}	0.0157
	J'_{zz}	0.014129	X'_{vr}	−0.02902
	Y'_{β}	0.27947	$Y'_{\beta\beta}$	0.66366
	Y'_{r}	0.05243	Y'_{rr}	0.04036
	$Y'_{\beta\beta r}$	0.0917	$Y'_{\beta rr}$	0.4966
	N'_{β}	0.13028	$N'_{\beta\beta}$	−0.0685
	N'_{r}	−0.03526	N'_{rr}	−0.02426
	$N'_{\beta\beta r}$	−0.1567	$N'_{\beta rr}$	−0.06383
	C_{TM}	$0.007245 - 0.0333Fn + 0.105267Fn^2$		
Propeller	t_p	0.34	w_{p0}	0.434
	x'_P	−0.5	C_1	0.271
	C_2	−0.1155	C_3	−0.34
Rudder	x'_R	−0.53075	γ_R	0.6
	kx	0.52	ε	1.3
	Lr'	−1.0	C_{R1}	0.7934
	C_{R2}	4.1921	t_R	0.4607
	x_H	−2.1257	a_H	$-1.2986Jp^2 + 1.0151Jp$
	C_{RS1}	−0.000201	C_{RS2}	0.0192
	C_{RS3}	0.644	C_{RP1}	−0.000227
	C_{RP2}	−0.0307	C_{RP3}	0.336

model with the Mariner rudder. The model ship with the Mariner rudder has slightly better turning ability and course stability, but the model with the MSV rudder also has sufficient maneuverability. However, unlike for the Mariner rudder, for the MSV rudder, within existing stern designs, there is scope for further improving the ship's maneuverability by increasing the size of MSV rudder. This is because, for the MSV rudder, there is sufficient clearance for an increased rudder area available both between the rudder bottom plate and the ship's keel and between the rudder top plate and the ship's hull.

2. A simulation of a VLCC with an MSV rudder was developed. Using the concept of mean flow speed around the rudder, the mathematical model of the MSV rudder was improved by referring to the results of the free-running tests.
3. An optimized MSV rudder position is proposed to reduce the unsymmetrical maneuvering motion of a ship with an MSV rudder.

Appendix

The values of hydrodynamic coefficients that were used in the simulation are shown in Table 4.

References

1. Duvigneau R, Visonneau M, Deng GB (2003) On the role played by turbulence closures in hull shape optimization at model and full scale. J Mar Sci Technol 8:11–25
2. Kim YB, Goo JS (2004) An anti-wind-up controller design based on a two-degrees-of-freedom servosystem design approach. J Mar Sci Technol 8:169–176
3. IMO MSC 76/23 (2002) Resolution MSC.137(76), standards for ship manoeuvrability. Report of the maritime safety committee on its seventy-sixth session, annex 6. International Maritime Organization
4. DNV (1985) Hull equipment and appendages: stern frames, rudders and steering gears. Rules for classification of steel ships, part 3. Det norske Veritas, Norway, Chapt. 3, Sect. 2:2–19
5. Nabeshima K, Omote M, Ueno A, et al (1997) A new type rudder, VecTwin, and the actual results of its manoeuvring performance (in Japanese). J Kansai Soc Nav Archit 228:157–165
6. Nomoto K, Karasuno K (1969) A new procedure of maneuvering model experiment (in Japanese). J Soc Nav Archit Jpn 126:131–140
7. MMG (1980) MMG report V (in Japanese). Bull Soc Nav Archit Jpn 616:565–576
8. Hasegawa K (1980) On a performance criterion of autopilot navigation. J Kansai Soc Nav Archit 178:93–104
9. Kijima K, Nakiri Y (2002) On the practical prediction method for ship manoeuvring characteristics (in Japanese). Trans West Jpn Soc Nav Archit 105:21–31
10. Hamamoto M, Enomoto T (1997) Maneuvering performance of a ship with Vec twin rudder system. J Soc Nav Archit Jpn 181:197–204
11. Kawamura T, Miyata H, Mashimo K (1997) Numerical simulation of the flow about self-propelling tanker models. J Mar Sci Technol 2:245–256
12. Ohmori T, Fujino M, Miyata H (1998) A study on flow field around full ship forms in maneuvering motion. J Mar Sci Technol 3:22–29
13. Yuda N (1999) Experimental study on hydrodynamic forces acting on the Vec twin rudder system (in Japanese). J Jpn Inst Navig 102:71–77
14. Kose K, Hosokawa M, Yamada H, et al (1992) A study on performance estimation of special rudders (in Japanese). Trans West Jpn Soc Nav Archit 84:49–57